Optical Chopper for LOngitudinal-Detected (LOD) EPR

Utsab Banerjee[a,1,#], Zhenfeng Pang[a,1], Thanh Phong Lê [b], Andrea Cappozi[b,c], and Kong Ooi Tan[a,*]

[a]Laboratoire des Biomolécules, LBM, Département de Chimie, École Normale Supérieure, PSL University, Sorbonne Université, CNRS, 75005 Paris, France

[b]LIFMET, Institute of Physics, École polytechnique fédérale de Lausanne (EPFL), Station 6, 1015 Lausanne, Switzerland

[c]HYPERMAG, Department of Health Technology, Technical University of Denmark, Building 349, 2800 Kgs Lyngby, Denmark

[#]Present address: Department of Chemistry, TUM School of Natural Sciences, Technical University of Munich, 85748 Garching, Germany

[1]Denotes equal contributions

*Corresponding Author:

Kong Ooi Tan
Laboratoire des Biomolécules, LBM, Département de Chimie,
École Normale Supérieure, PSL University, Sorbonne Université, CNRS,
75005 Paris, France
ORCID:0000-0002-3094-3398
E-Mail: kong-ooi.tan@ens.psl.eu

Keywords: Dynamic Nuclear Polarization (DNP), High-field Electron Paramagnetic Resonance (EPR), NMR, Optical Chopper, Lock-In Detection, Gyrotron

Abstract

Dynamic nuclear polarization (DNP) is a nuclear magnetic resonance (NMR) hyperpolarization technique that mediates polarization transfer from unpaired electrons to nuclear spins. DNP performance can vary significantly depending on the types of polarizing agents employed, and the criteria for optimum DNP efficiency are not fully understood. Thus, a better understanding of the structure, electron paramagnetic resonance (EPR) linewidths, and relaxation properties would aid in designing more efficient DNP polarizing agents. However, EPR characterizations of the polarizing agents are typically performed in different environments (e.g., strength of magnetic field and microwave power) than typical DNP experiments. Here, we demonstrate a low-cost and home-built setup that enables *in-situ* EPR detection in a dual resonance DNP-NMR/EPR probe using an optical chopper. The chopper modulates the microwave irradiation, thereby modulating the longitudinal magnetization (M_z) of the electron spins. Our results of DNP and EPR spectra on TEMPOL using a solid-state microwave source at 6.7 T / 188 GHz and 4.2 K showed a good agreement. In principle, an optical chopper should be compatible with a wide range of microwave sources, including gyrotrons that output high-power microwaves. To verify this, we placed an optical chopper in between the waveguides of a 527 GHz gyrotron and successfully reproduced a DNP field profile similar to the case without a chopper. Hence, our work provides a proof-of-principle setup that could enable a gyrotron-based EPR spectrometer in the future.

1. Introduction

Dynamic nuclear polarization (DNP)[1–3] is an NMR hyperpolarization technique widely applied in studying materials and biological macromolecules, including catalysts, battery materials, fibrils, membrane proteins, etc.[4,5] In DNP, polarization is transferred from unpaired electrons, borne on either organic radicals or paramagnetic metal ions, to nuclear spins. However, the actual DNP performance varies significantly depending on factors such as magnetic field strength, types of radicals, solvents, temperatures, target molecules, etc. For instance, we have recently investigated ^{1}H-DNP enhancement factor ε on amyloid fibrils at 18.8 T,[6] and the results vary significantly (ε~6-50) depending on the type of biradicals employed. Moreover, these numbers are considerably low if compared to the theoretical limit of ε~658. To improve DNP performance, it is essential to characterize the radicals' spin parameters, such as *g* tensors, relaxation times, electron-electron coupling strengths, etc., to design more efficient DNP polarizing agents. [7–11] Nevertheless, unambiguously determining some of these parameters (for instance, *g* tensors) is challenging without high-field EPR spectrometers that confer high resolution. Combining experimental data obtained at lower fields with multifrequency EPR measurements and fittings can characterize these radicals with higher accuracy.[9] Besides that, it has been reported that the electron relaxation times T_{1e}, a crucial factor affecting the DNP performance,[10,12] of several organic radicals unexpectedly decrease as the magnetic field increases.[13,14] However, most commercial EPR spectrometers are limited to magnetic fields lower than standard DNP machines. Hence, this justifies the need for *in-situ* EPR characterization of polarizing agents at the same DNP conditions.[15]

While various strategies exist for designing dual-resonance DNP-NMR / EPR probe,[16–22] we adopted the LOngitudinal-Detected (LOD) EPR scheme due to its (1) general applicability to microwave (μw) sources with almost any frequencies and power, (2) affordable cost, and (3) relatively easy implementation with minimal modification needed for our existing DNP setups.[18,19,23–28] In typical LOD-EPR experiments, the longitudinal magnetizations of electron spins are driven to oscillate periodically along the *z*-axis by turning the μw on/off. The *z*-magnetization (M_z) decreases when the EPR transition is saturated by μw and recovers via spin relaxation when the μw are turned off. If the μw source is periodically turned on/off, the resulting time-dependent M_z (t) induces a voltage across a pickup coil placed along the *z*-axis, [19,23,29,30] which is measured as an EPR signal. A key advantage of this detection scheme is that the induced

EPR signal can be set to oscillate at a modulation frequency much lower than the electron Larmor frequency, allowing detection of ~GHz EPR transitions in the audio frequency (~kHz) range. Thus, LOD-EPR detection obviates the need for high-frequency μw accessories (switches, receivers, and amplifiers) that are not readily available and expensive. The method has been demonstrated on various dissolution DNP setups (3.35 T-7 T) by directly triggering the solid-state μw source on/off.[18,19,25,27,31] While it is trivial to modulate the μw power generated from the solid-state sources using either voltage-controlled attenuators or electrical switches, such methods cannot be easily applied to high-power sources like gyrotrons because the abovementioned μw accessories are usually rated for operations at low powers ($<$ 1 W).

Thus, we propose a new LOD-EPR design that does not require sophisticated μw accessories and could potentially be applied on gyrotrons for EPR detection. This can be achieved by using an optical chopper, whose rotating metallic blades periodically block the μw beams, thereby modulating the μw amplitudes similar to gating of the μw source. Then, the following detection scheme remains similar to the conventional LOD-EPR scheme, i.e., the induced voltage V(t) across the LOD solenoid coil can either be directly observed on an oscilloscope or mixed with the optical chopper reference signal in a lock-in amplifier. The deployment of an optical chopper is inspired by the quasi-optical setup installed in NHMFL (Florida), which incorporates a mechanical shutter that allows a gyrotron to be shared between two NMR spectrometers.[32] It was also demonstrated in another study that an optical chopper can be used to characterize the μw beams generated from gyrotrons or solid-state sources.[33,34]

As a proof of principle, we first demonstrated how a modular LOD-EPR coil was retrofitted to the existing 6.7 T dissolution DNP setup (**Fig. 1**) in our lab,[18,31] to achieve an *in-situ* dual resonance DNP-NMR (^{1}H Larmor of 285 MHz) / EPR (188 GHz) detection. Then, we showed the experimental setup and the results of an optical chopper LOD-EPR. Finally, we demonstrated that the optical setup is compatible with a 527 GHz gyrotron by showing the results of DNP experiments.

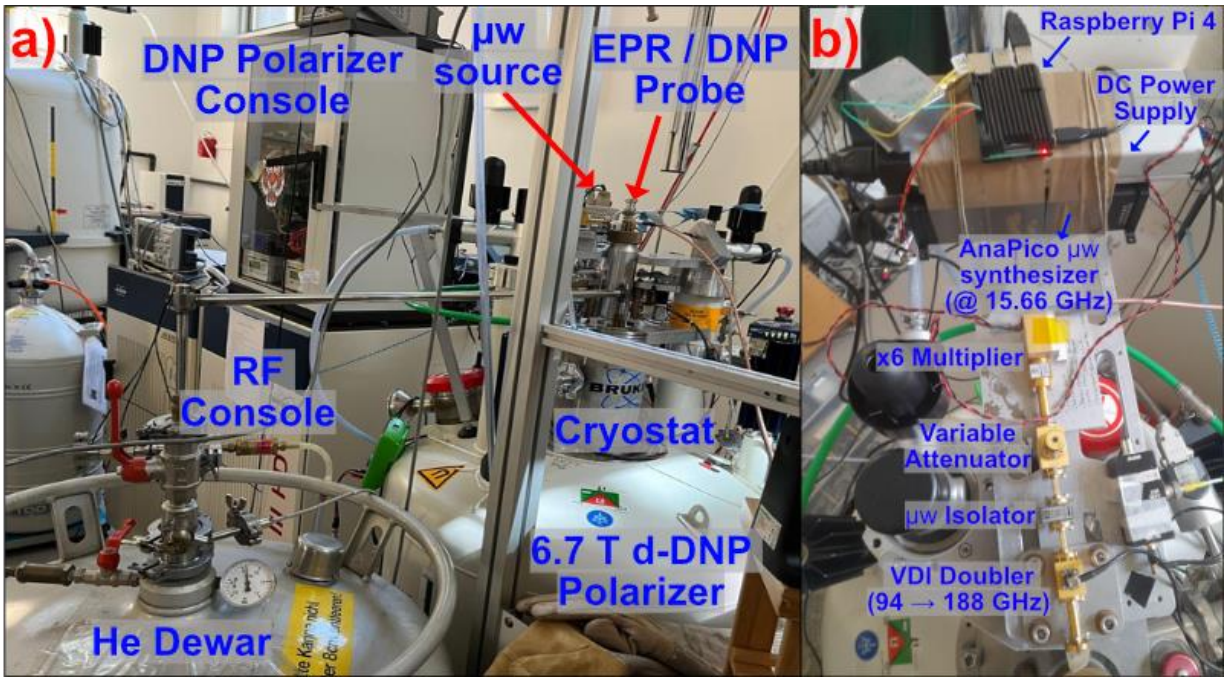

Figure 1: Photograph of the (a) 6.7 T DNP spectrometer and the (b) 188 GHz µw source.

2. Materials and Methods

2.1. Sample Preparation

All EPR / DNP experiments at 6.7 T were performed using 50 mM TEMPOL (Sigma Aldrich) dissolved in DNP juice (d_8-glycerol/D_2O/H_2O in a 5:4:1 ratio by volume). About 200 µL of the sample was pipetted into the sample cup (**Fig. 2a**). For the DNP experiment at 18.8 T, we prepared ~40 mM of BDPA (Sigma Aldrich) in a 1:1 mixture (by volume) of hexafluorobenzene and toluene. The BDPA sample was then packed into a 10 mm NMR tube.

2.2. Dissolution DNP (6.7 T/ 188 GHz/ 285 MHz) Spectrometer

The 6.7 T dissolution DNP polarizer was provided by Bruker BioSpin to ENS,[31] and the cryostat prefilled with liquid helium can be cooled down to 1.2 K upon pumping to ~ 1 mbar.[35,36] All temperature and pressure diagnostics and controllers, as well as the helium level indicator, are embedded in the DNP polarizer console (**Fig. 1a**). The microwave is generated from a synthesizer (AnaPico, model APUASYN20) at 15.66 GHz (**Fig. 1b**), which is then up-converted to 94 GHz by a 6x frequency multiplier (RPG-Radiometer Physics GmbH). Then, a variable attenuator was used to manually control the µw power that enters the frequency doubler (Virginia Diodes Inc., model D200) and the final output power of the ~188 GHz microwave frequency is ~28 mW before being

delivered to the probe. A stainless-steel circular microwave waveguide was used in the DNP probe to achieve good thermal insulation. Nevertheless, stainless steel has poor electrical conductivity, and, hence, results in a lossy (~ 10 dB) μw transmission. We have measured ~ 1 mW of μw power at the sample position using a power meter (Ophir Optronics, model 3A-P-THz) at room temperature. The μw frequency and amplitude generated from the AnaPico synthesizer can be controlled directly from a GUI software provided by the manufacturer or a Raspberry Pi 4.

2.3. Dual Resonance LOD-EPR (188 GHz) and DNP-NMR (285 MHz) Probe

A custom-built LOD-EPR probe (**Fig. 2a**)[18] was adapted into an existing dissolution DNP probe. The two components were integrated by using a 3D-printed adaptor (Ender-3 S1 Pro, Creality) that couples the dynamic seal region of the EPR probe to the top part of the DNP probe (**Fig. 2b**). Then, the EPR coil made from 600-turn 0.1 mm copper wire is positioned such that the window faces the μw reflector (**Fig. 2e**). The total resistance of the coil is ~30 Ω at room temperature or ~ 1.2 Ω at 4.2 K. The EPR coil is enclosed with an NMR rf insert (**Fig. 2d**), which is inductively coupled to a sniffer coil. The NMR saddle coil can be fabricated by using either laser or direct CNC machining, and it is soldered to non-magnetic ceramic capacitors (Johanson Technology, Inc) to achieve a resonance frequency of ~ 285 MHz for ^{1}H NMR detection. The NMR coil was fixated on a standard 10 mm NMR borosilicate glass tube (cut with a diamond wheel) using either microwave-transparent Kapton or Teflon tape. The final assembly (**Fig. 2f**) allows both DNP-NMR and EPR detection in a single setup, i.e., an *in-situ* EPR measurement under the same environment as DNP experiments.

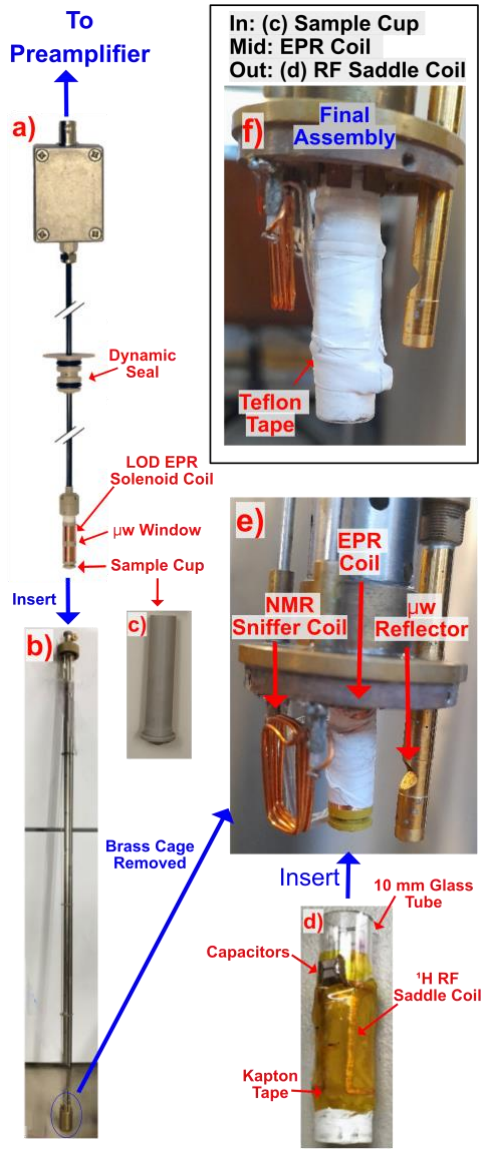

Figure 2: Photographs of the (a) LOD-EPR probe, (b) dissolution DNP probe, (c) sample cup, (d) NMR rf saddle coil, (e) zoomed-in sample region, and (f) the final assembly featuring the sample cup inside the LOD-EPR coil, which is inside the RF saddle coil. Figure (a) was extracted with permission from Lê et. al.[18]

2.4. Standard LOD-EPR Detection

The setup of a standard LOD-EPR detection via modulation of μw power using electrical switching will be briefly discussed here. It is known that the LOD detection is, in general, less sensitive than the conventional continuous-wave (CW) technique. Moreover, the low-frequency (< 10 Hz) detection strategy in our LOD setup is severely susceptible to noise from vibration and electrical grid, i.e., harmonics of 50 Hz AC noise. Hence, the induced voltage in the LOD-EPR coil is pre-amplified by 10,000x using a differential amplifier (AD8421, Analog Devices) and filtered via a homebuilt 10 Hz low-pass filter comprised of a simple RC (resistor-capacitor) network. Note that the preamplifier is powered by a 9 V battery (**Fig. 3**) to avoid AC noise from the grid. Then, the signal is digitized by a USB-6001 data acquisition device (DAQ) from National Instruments (NI), which performs digital lock-in detection in LabVIEW.[18,30] Alternatively, the signal can be acquired using an oscilloscope (EDUX1052A, Keysight), which can average a maximum of 65536 scans. We usually use the oscilloscope in the initial setup (for easier troubleshooting if signal is not observed), before switching to the DAQ with lock-in detection for better sensitivity. Although the oscilloscope directly displays the LOD-EPR waveform (**Fig. S1**) that allows the extraction of the electron relaxation times (T_{1e}), we switched to the DAQ because the oscilloscope connected to the electrical grid is susceptible to the 50 Hz AC noise. The μw power is modulated by triggering the frequency synthesizer (AnaPico) with transistor-transistor logic (TTL) pulses from either the DAQ or a function generator (JT-JDS6600, Joy-IT).

2.5. Optical Chopper and Lock-In Amplifier for LOD-EPR

Apart from the same probe and preamplifier discussed in the previous section, we used a commercial optical chopper (SR540) and a lock-in amplifier (SR 860) from Stanford Research Systems (**Fig. 3**). The optical chopper has a maximum chopping frequency of 400 Hz for the 5/6-slot blade or 3.7 kHz if the 25/30-slot blade is employed. The 5/6-slot blade made from anodized aluminum can reflect μw and it has a slot width of ~ 21 mm, which is sufficiently large compared to the μw waveguides (~4.5 mm at 188 GHz and ~ 17 mm at 527 GHz).[37] Instead of using the RC low-pass filter, we used the filter incorporated inside the commercial lock-in amplifier. The optical chopper and the lock-in amplifier constitute an integrated commercial setup that is readily interfaced and commonly employed for laser beam diagnosis. The settings of the lock-in amplifier used are detailed in Table 1. Throughout the experiment, we engaged the 'Auto Phase' function on the lock-in amplifier and recorded the absolute-value component of the demodulated signal as the EPR intensity. Following adjustments to the μw frequency, we allowed ~ 1 minute for the experimental setup to stabilize. Note that the optical chopper is always placed at 45° with respect

to the direction of μw propagation to minimize reflection back to the μw source. Furthermore, it is known that the μw diffracts and loses power in the absence of waveguides. Hence, we performed DNP in the absence of both waveguides and optical chopper, i.e. in open air, to ensure that there is still sufficient μw power to saturate the electron spins. This is justified by the fact that DNP is observed if the electron spins are partially, if not fully, saturated.

Filter	24 dB/octave
Input Range	300 mV
Time Constant	300 ms
Sensitivity	200 mV
Ground	Float
Couple	AC
Source	Chop
External	Positive TTL

Table 1 Settings of the SRS lock-in amplifier used in the LOD-EPR experiments.

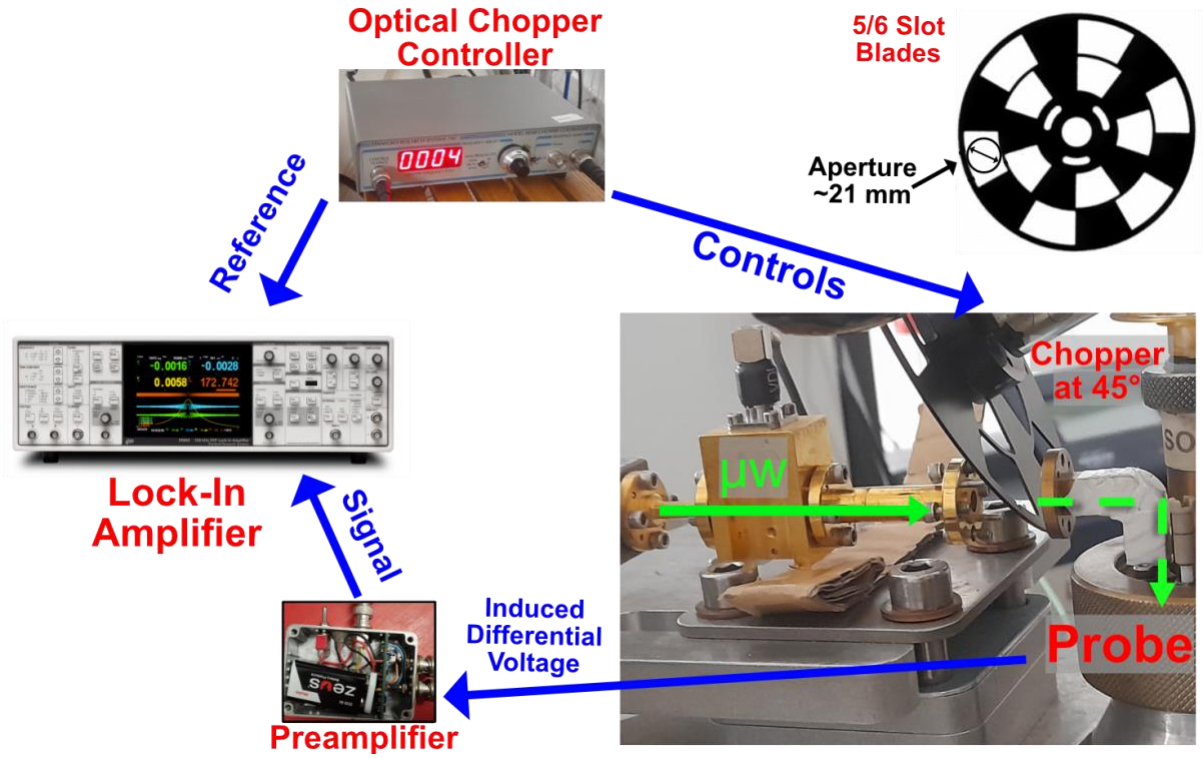

Figure 3: Schematic diagram of the optical chopper EPR setup at 6.7 T, which sinusoidally modulates the μw power for LOD-EPR detection.

2.6. 18.8 T / 527 GHz / 800 MHz Gyrotron-DNP Spectrometer

Our lab hosts a commercial (Bruker) 18.8 T magic angle spinning (MAS) DNP Spectrometer equipped with a 527 GHz gyrotron, a field-sweepable superconducting magnet (range of ± 52 mT or ± 2 MHz on ^{1}H), a 3.2 mm HXY MAS DNP probe, and a nitrogen-based heat exchanger that can cool the sample to ~ 100 K under MAS (or ~ 80 K in static) condition.[6] A section of the waveguides was removed (**Fig. 6**) to facilitate the installation of the optical chopper. To bypass the interlock mechanism (a failsafe system) inherent in the gyrotron system, the waveguide was sealed with μw-transparent Kapton tape (to prevent N_2 gas leakage) and a 470-Ω resistor (**Fig. S2**) was connected at the gyrotron interlock (to mimic a low-temperature probe environment). For DNP NMR measurements, we used a Bruker MAS probe, but the stator that was replaced with a 3D-printed housing that can accommodate a cut NMR tube (**Fig. S3**).

2.7. DNP-NMR and LOD-EPR Spectroscopy at 6.7 T

All experiments were performed at 4.2 K and a pressure of ~ 980 mbar to minimize helium consumption. The DNP experiments were performed with 28 mW μw power without frequency modulation. The ^{1}H saturation pulses were applied only once before acquiring the first data point in the DNP frequency profile. Subsequently, a one-minute delay was waited before changing the μw frequency, and the ^{1}H spectrum was acquired by using a small flip angle (5°) pulse. All EPR experiments were acquired with a 5 Hz modulation frequency, which yields an optimal signal for TEMPOL.

2.8. DNP-NMR Spectroscopy at 18.8 T

All DNP experiments were performed at 100 K. However, we observed a superposition of narrow liquid-state and broad solid-state spectrum if excess μw power was used, which suggested a non-uniform temperature distribution across the sample since only part of the static (non-spinning) sample was exposed to the μw. Hence, determining the DNP enhancement factor by comparing the NMR spectrum under μw on/off condition was unreliable. The DNP experiments were performed using a gyrotron operating with a collector current of 110 mA and at a μw frequency of 526.98 GHz, which is on resonance with the BDPA radical (g_{iso} = 2.00264 at B_0 = 18.801 T)[38] to mediate the Overhauser DNP effect. A DNP build-up time of 5 s was used prior to NMR acquisition.

3. Results and Discussion

3.1. Dual Resonance LOD-EPR and DNP-NMR Setup at 6.7 T

Figure 4 shows the results obtained using the *in-situ* dual resonance DNP-NMR / EPR setup (**Section 2.3**), where both DNP-NMR and EPR data were adjacently acquired in the same experimental session without changing the sample or probe. It showcases a typical DNP frequency profile exhibited by TEMPOL, where a maximum positive or negative DNP transfer is observed at ~187.95 GHz or ~ 188.4 GHz, respectively, when off-resonance microwave irradiation around or slightly less than ^{1}H NMR Larmor frequency $\upsilon_{0\mathrm{H}} = 285$ MHz is applied.[27,39,40] To better analyse the DNP profile, we introduce a derivative DNP profile (red plot in **Fig. 4a**), derived from the first derivative of the DNP frequency profile (blue plot in **Fig. 4a**) using a 30 MHz modulation in EasySpin.[41] Analysis via a derivative spectrum is a common technique in continuous-wave (CW) EPR spectroscopy as it can unveil fine features that may not be evident in the integrated spectrum. The LOD-EPR (**Fig. 4b**) spectra were obtained by modulating μw power using electrical switching while the signal was acquired either using the DAQ (NI) with a low-pass filter or solely the SRS lock-in amplifier.

We observed that LOD-EPR spectrum acquired using the DAQ setup is rather broad or featureless. We speculated that the finite response time of the electrical components in the home-built low-pass filter could influence the EPR spectrum. To confirm our hypothesis, we replaced the analog filter and the DAQ setup (with a digital filter in the software) with an advanced commercial lock-in amplifier (SRS), which indeed yields a higher-resolution EPR spectrum with finer features. We simulated an EPR spectrum of TEMPOL (**Fig. 4b**) using EasySpin (see Supporting Information) to fit the experimental results.[41] The fitted results yield g = [2.00878, 2.00584, 2.00204], which is similar to the values reported in the literature. A small deviation (less than 0.001) was not unexpected because a different concentration and solvent were used here.[42]

Upon comparing the results of the DNP and EPR spectra, it is evident that the full breadths (~ 800 MHz at ~ 10 % height) of both spectra align well. Moreover, dashed line ④ marks the μw frequency at which the DNP zero-crossing (or the most negative value in the derivative DNP) occurs, closely matching with the EPR g_{yy} peak. Note that the DNP zero-crossing may not perfectly coincide with the EPR g_{yy} peak due to the asymmetric nature of the EPR spectrum of TEMPOL. This is supported by the observation that the positive DNP condition usually yields a higher ^{1}H NMR signal than the negative DNP condition. Besides that, the μw power generated from the source is not uniform across frequencies, with a 5-10 % deviation in power expected according to specifications. Additionally, the ^{1}H-DNP intensity shown in **Fig. 4a** may not have reached a steady state because the profile was acquired with a short delay between each frequency point (see Section 2.7), and the ^{1}H pre-saturation pulses were applied only once

throughout the profile. This issue could be addressed by repeating the experiment with more saturation and longer delays, but it will be too time- and helium-consuming. These factors may account for the slight mismatch between the DNP and EPR spectra.

Three frequency steps were observed in the integrated DNP frequency profile (or three peaks in the derivative spectrum marked with ①, ②, and ③), which again correlate well with the steps observed in the EPR spectrum (red plot in **Fig. 4b**). These steps clearly feature the well-known electron-^{14}N hyperfine splittings along the A_{zz} axis,[43] where the line ② marks the $m_I = 0$ manifold of the ^{14}N nucleus, as well as the g_{zz} position of the EPR spectrum. Moreover, our results corroborate well with the simulated EPR spectrum (magenta plot in **Fig. 4b**) using the A_{zz} values (~ 100 MHz) reported in the literature.[42]

Line ⑤ indicates the frequency at which the optimal negative DNP condition (or zero in the derivative DNP) occurs. For the cross effect and thermal mixing DNP mechanisms, DNP occurs when the frequency difference between the μw-saturated electron and the non-saturated second electron matches the nuclear Larmor frequency.[44,45] Moreover, the DNP efficiency is proportional to the polarization difference and the electron spin density (n_e per unit B_0 field) between the two electrons. For nitroxide, the negative ^{1}H-DNP condition (line ⑤) typically aligns closely to the g_{xx} position in the EPR spectrum because the frequency difference between the most populous g_{yy} and the g_{xx} line is determined by the equation:

$$\Delta v = \left(g_{xx} - g_{yy}\right)\beta B_0/h \qquad (1)$$

where the equation governing the EPR frequency ($hv = g\beta B_0$) is used; β and h are the Bohr magneton and the Planck's constant, respectively. By substituting the g values determined earlier into Eq. (1), one obtains ~ 276 MHz, closely matching the ^{1}H Larmor frequency of 285 MHz at 6.702 T. Note that the relation generally holds true for most high-field DNP experiments using nitroxides as the value of $(g_{xx} - g_{zz})\beta/h = 41.1485$ MHz/T is akin to the gyromagnetic ratio of ^{1}H $\gamma_{1H}/2\pi = 42.5775$ MHz/ T. Again, the LOD-EPR spectrum measured using the dual-resonance DNP / EPR probe confirms that line ⑤ indeed coincides with the predicted g_{xx} line. With the establishment of a reliable LOD-EPR setup that remarkably complements the DNP spectrometer, we proceeded to implement the optical chopper EPR setup.

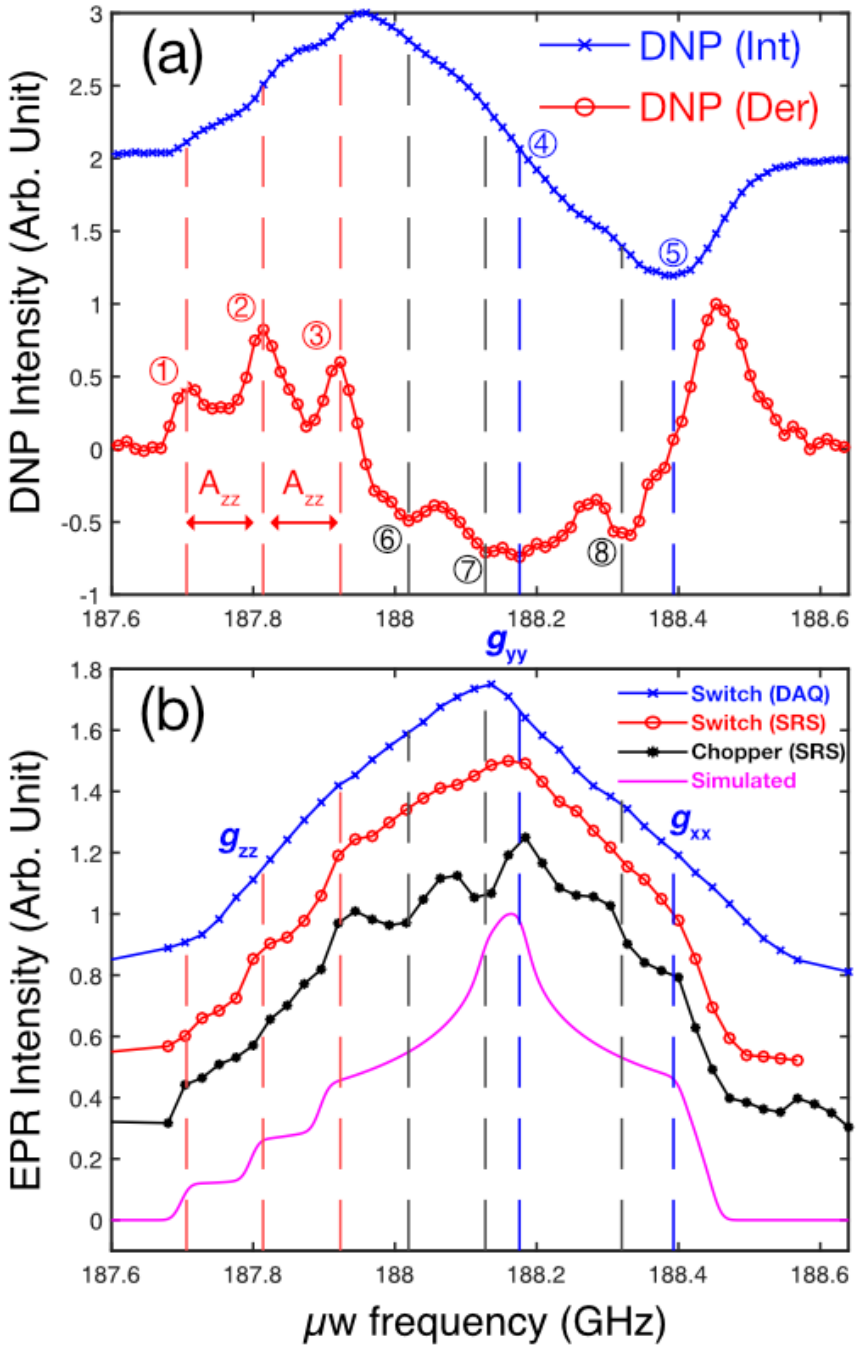

Figure 4: The results of (a) a standard or integrated DNP frequency profile (blue) with its' derivative (red) and (b) LOD-EPR curves of TEMPOL in DNP juice at 6.702 T and 4.2 K. The μw power was modulated by either electrical switching (blue and red) or an optical chopper (black), and the signal was measured by either the DAQ (blue) or SRS lock-in amplifier (red and black). A simulated plot of EPR (magenta) is shown here for comparison. All intensities are normalized with respect to the positive maximum values. The intensity of the DNP (blue) and measured EPR profiles in (b) are offset in the *y*-axis for easier comparison. The first three numbered red dashed lines (--) at ①187.706, ②187.814, and ③187.923 GHz indicate the ^{14}N hyperfine splittings of A_{zz} ~ 100 MHz. The blue dashed lines at ④188.1758 and ⑤188.393 GHz mark the DNP zero-crossing (EPR g_{yy} value) and the negative DNP condition (EPR g_{xx} value), respectively. The grey dashed lines (⑥188.0192, ⑦188.1276, and ⑧188.32 GHz) mark the local minima in the derivative DNP plot.

3.2. Optical Chopper LOD-EPR at 6.7 T

Instead of modulating the μw power with electrical switching for LOD-EPR detection, a similar objective can be achieved by using an optical chopper that mechanically transmits or reflects the μw irradiation. To safeguard the microwave frequency doubler (VDI) from potential damaged caused by the reflected μw, the optical chopper was installed at 45° (see Section 2.5) in between the waveguides. The chopper was set to chop at 5 Hz, which corresponds to ~ 1 Hz rotation on a 5/6-blade disc (see the slow-motion video in Supporting Information).

The EPR spectrum acquired using the optical chopper (black plot in **Fig. 4b**) exhibits a comparable linewidth, peak position, and the fine A_{zz} splittings to the other EPR spectra. However, noticeable differences are observed around the g_{yy} position, particularly those marked by dashed lines ⑥ and ⑦. A possible explanation for these differences is that the sinusoidal modulation of μw power using the chopper blades generates a different waveform in the induced EPR voltage compared to square pulses used in electrical switching. When square μw pulses are applied, electrons have sufficient time (**Fig. S1**) for full relaxation or saturation (assuming adequate μw power), resulting in EPR signals closer to actual thermal equilibrium. Conversely, electrons subject to sinusoidal μw irradiation reach a quasi-static thermal equilibrium with nearby ^{1}H nuclear spins that are inadvertently polarized by DNP during the LOD-EPR experiments. Our hypothesis is supported by the need to wait for at least a minute between each μw frequency point during the LOD-EPR experiment (see **Section 2.5**), allowing nearby ^{1}H spins to be polarized by DNP and reach an equilibrium with the electron. Moreover, the frequency difference between the troughs or local minima (⑥ and ⑦) and the hyperfine-induced frequency steps (① and ②) coincidentally matches the ^{1}H Larmor frequency of 285 MHz, i.e., ⑥-① = ⑦-②=313 MHz. Unsurprisingly, the frequency difference between the troughs (⑦-⑥) is 108 MHz, which is close to the A_{zz} ~ 100 MHz reported earlier. Such fine features can also be inferred from the derivative DNP profile, where positions ⑥ and ⑦ also exhibit local minimal values, implying a significant change in the DNP profile or EPR line (as agreed in the observed LOD-EPR spectrum).

A similar correspondence is observed on line ⑧, where a local minimum in the derivative DNP profile coincides with a sudden signal drop in the LOD-EPR spectrum. Hence, we conjecture that the operating principle of the optical chopper LOD-EPR method can be applied to better understand the actions of the DNP polarizing agents in the actual DNP condition. These effects may be less prominent in conventional CW or pulsed EPR experiments due to insufficient μw power (for CW EPR) or pulse duration (for pulsed EPR) to enable efficient DNP, thus failing to establish quasi-equilibrium between electrons and hyperpolarized nuclei.

Another reason contributing to differences between LOD-EPR spectra may be the transmission of lower averaged μw power in the optical chopper setup due to diffraction in the gap between waveguides. Consequently, electron spins may be less efficiently saturated, resulting in differently affected LOD-EPR signals influenced by the electron-electron spectral diffusion in the high-concentration (50 mM) TEMPOL sample.[46] Although more points could be sampled in EPR experiments and the signal-to-noise improved with additional scans, critical helium supply shortages prevented further experiments. Alternatively, attempts were made to conduct LOD-EPR experiments using cryogen-free magnets,[39] but low-frequency vibration from the pulse tube (PT) cryocooler interfered severely with measurements. This issue may be mitigated by employing higher modulation frequencies and temperatures.[25] Various detection strategies are currently under investigation, although discussion thereof is beyond the scope of this work.

3.3. Compatibility of Optical Chopper with 527 GHz Gyrotron

We hypothesize that the optical chopper setup could be adapted for high-power μw sources such as gyrotrons, resulting in a gyrotron-based EPR (GyroEPR) spectrometer. Note that the manufacturer of the gyrotron (Communications and Power Industries, Palo Alto) had exposed the gyrotrons to 100 % reflection for at least an hour, and no fault or damage was observed.[47] Thus, we performed DNP experiments using a gyrotron incorporated with an optical chopper in between the waveguides (**Fig. 5a**) . Figure **5b** shows that the DNP field profiles on BDPA with or without the chopper are very similar, with the maximum Overhauser DNP intensity observed at the same B_0 field.[48–51] Moreover, the DNP spectrum acquired with a chopper exhibits ~33 % less signal, as some μw power was lost due to reflection and diffraction. In conclusion, the two-hour DNP experiments further confirms that the optical chopper does not damage or adversely affect the fundamental operation of a gyrotron.

Motivated by these promising results, we have installed an LOD-EPR coil into the probe (**Fig. S3**) and attempted to acquire LOD-EPR signal. A faster chopper frequency of 100 Hz was chosen because the commercial DNP probe can be cooled down to only ~ 100 K, where the electron relaxation rate is likely faster than in the previous experiment performed at 4.2 K. However, no EPR signal was observed, potentially due to (1) ~6x lower electron Boltzmann population than the condition at 6.7 T and 4.2 K, (2) severe vibration noise from the high-flow cooling N_2 gas, and (3) a less sensitive LOD-EPR coil as the resistance of copper wire increases at higher temperatures. These issues could potentially be resolved if the sample can be cooled down to a lower temperature ≤ 10 K, and such a system is currently under construction in our lab.

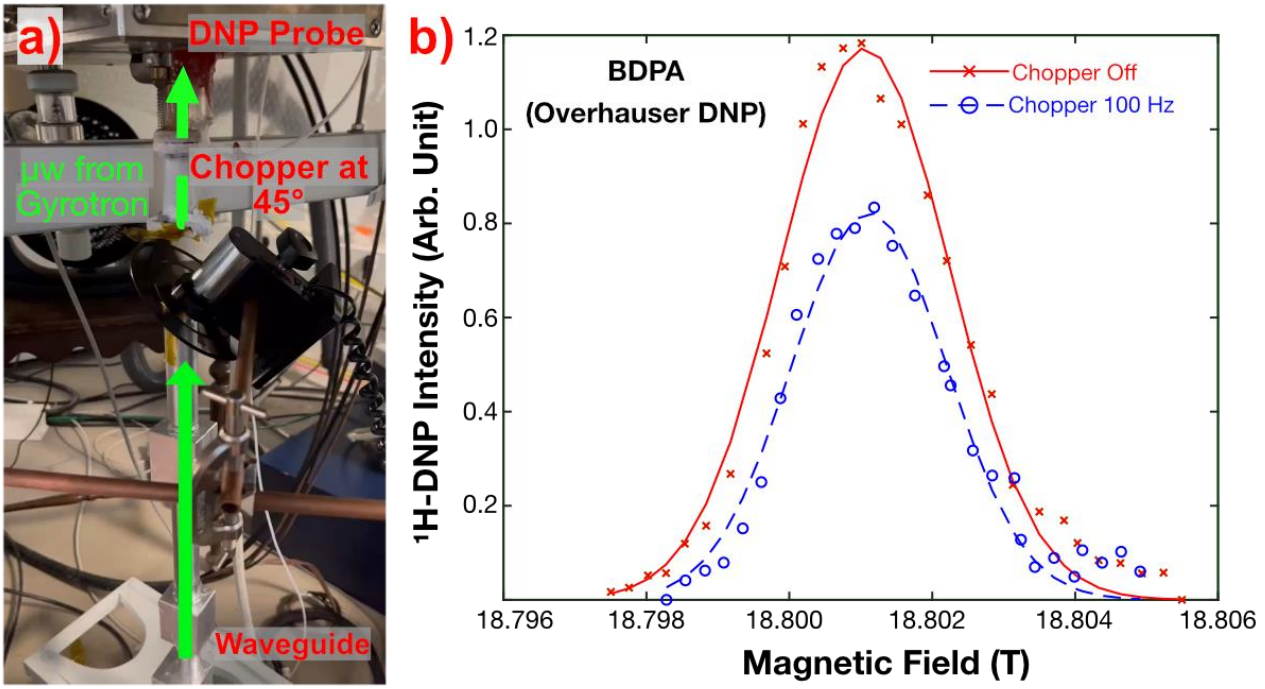

Figure 5: (a) Photograph of an optical chopper interfaced with a 527 GHz gyrotron. (b) ^{1}H-DNP field profile of BDPA with the optical chopper (a) turned off or (b) spinning at 100 Hz. Both data were fitted with Gaussian curves for eye guidance. The experiments were performed using a commercial DNP probe in static (non-spinning) mode at ~100 K, and the MAS stator was replaced by a 3D-printed housing (see **Fig. S3**).

4. Conclusion and Outlook

We have demonstrated a dual resonance LOD-EPR / DNP-NMR setup that enables *in-situ* EPR detection in a 6.7 T DNP polarizer. The results of the DNP frequency profile and EPR spectrum allow us to analyze and better understand the DNP mechanism, confidently assigning the *g* values and hyperfine interactions of the radicals in the actual DNP environment. Hence, we believe that such a unique hardware allows for the characterization the DNP polarizing agents in the actual high-field DNP condition, potentially aiding in the design of more efficient DNP polarizing agents.[9,10,52,53] Moreover, it could facilitate a better understanding of the fundamental DNP mechanism involving a complex spin system.[54] On the other hand, high-field EPR spectroscopy offers a high resolution, particularly beneficial for studying Kramers' system (half-integer spins).[55,56] Additionally, we have established an LOD-EPR system using an optical chopper, which is in theory applicable to any DNP system, including the gyrotron-based DNP spectrometer. To confirm the compatibility of the optical chopper with a gyrotron, we have successfully performed DNP experiments while both the optical chopper and the gyrotron are simultaneously turned on.

Hence, our work provides a proof-of-principle setup that could enable a gyrotron-based EPR (GyroEPR) spectrometer in the future.

Acknowledgements

We would like to thank Dr. Mathieu Baudin, Dr. Vineeth Thalakottor, and Dr. Kirill Sheberstov for providing various instrumentation (cryogenics, probe, and electronic circuits) supports. We are grateful of Dr. Sun Un (CEA) for useful discussions and lending us the 94 GHz microwave source. This work was supported by fundings obtained from the French National Research Agency: *PulsedDNP* (ANR-20-ERC9-0008) and *HFPulsedDNP* (ANR-21-CE29-0019), as well as RESPORE (n° 339299). Andrea Capozzi acknowledges the support from the Swiss National Science Foundation SPARK grant (CRSK-2_190547, assigned to Capozzi) and the Swiss National Science Foundation Ambizione grant (PZ00P2_193276, assigned to Capozzi).

Supporting Information Available: Figure S1 shows the direct detection of the induced EPR voltage detection using an oscilloscope. Figure S2 shows the gyrotron interlock mechanism is bypassed by connecting a resistor. Figure S3 shows the modified DNP probe with the MAS stator replaced by a 3D-printed housing. A slow-motion video that shows the operation of an optical chopper is available.

References

[1] A. S. Lilly Thankamony, J. J. Wittmann, M. Kaushik, B. Corzilius, *Prog. Nucl. Magn. Reson. Spectrosc.* **2017**, *102–103*, 120–195.

[2] A. Abragam, M. Goldman, *Reports Prog. Phys.* **1978**, *41*, 395–467.

[3] T. Wenckebach, *Essentials of Dynamic Nuclear Polarization*, Spindrift Publications, **2016**.

[4] B. Reif, S. E. Ashbrook, L. Emsley, M. Hong, *Nat. Rev. Methods Prim.* **2021**, *1*, 2.

[5] M. J. Duer, Ed. , *Solid-State NMR Spectroscopy Principles and Applications*, Wiley, **2001**.

[6] A. Lends, N. Birlirakis, X. Cai, A. Daskalov, J. Shenoy, M. B. Abdul-Shukkoor, M. Berbon, F. Ferrage, Y. Liu, A. Loquet, et al., *J. Biomol. NMR* **2023**, DOI 10.1007/s10858-023-00416-5.

[7] F. Mentink-Vigier, *Phys. Chem. Chem. Phys.* **2020**, *22*, 3643–3652.

[8] A. Equbal, S. K. K. Jain, Y. Li, K. Tagami, X. Wang, S. Han, *Prog. Nucl. Magn. Reson. Spectrosc.* **2021**, *126–127*, 1–16.

[9] J. Soetbeer, P. Gast, J. J. Walish, Y. Zhao, C. George, C. Yang, T. M. Swager, R. G. Griffin, G. Mathies, *Phys. Chem. Chem. Phys.* **2018**, *20*, 25506–25517.

[10] D. J. Kubicki, G. Casano, M. Schwarzwälder, S. Abel, C. Sauvée, K. Ganesan, M. Yulikov, A. J. Rossini, G. Jeschke, C. Copéret, et al., *Chem. Sci.* **2016**, *7*, 550–558.

[11] S. Chatterjee, A. Venkatesh, S. T. Sigurdsson, F. Mentink-Vigier, *J. Phys. Chem. Lett.* **2024**, 2160–2168.

[12] P. Niedbalski, C. Parish, Q. Wang, Z. Hayati, L. Song, A. F. Martins, A. D. Sherry, L. Lumata, *J. Phys. Chem. A* **2017**, *121*, 9221–9228.

[13] I. Tkach, I. Bejenke, F. Hecker, A. Kehl, M. Kasanmascheff, I. Gromov, I. Prisecaru, P. Höfer, M. Hiller, M. Bennati, *J. Magn. Reson.* **2019**, *303*, 17–27.

[14] D. Akhmetzyanov, H. Y. V. Ching, V. Denysenkov, P. Demay-Drouhard, H. C. Bertrand, L. C. Tabares, C. Policar, T. F. Prisner, S. Un, *Phys. Chem. Chem. Phys.* **2016**, *18*, 30857–30866.

[15] J. Granwehr, W. Köckenberger, *Appl. Magn. Reson.* **2008**, *34*, 355–378.

[16] A. A. Smith, B. Corzilius, J. A. Bryant, R. DeRocher, P. P. Woskov, R. J. Temkin, R. G. Griffin, *J. Magn. Reson.* **2012**, *223*, 170–179.

[17] K. Tagami, R. Thicklin, S. Jain, A. Equbal, M. Li, T. Zens, A. Siaw, S. Han, *J. Magn. Reson.* **2022**, 107351.

[18] T. P. Lê, J.-N. Hyacinthe, A. Capozzi, *J. Magn. Reson.* **2022**, *338*, 107197.

[19] J. Granwehr, J. Leggett, W. Köckenberger, *J. Magn. Reson.* **2007**, *187*, 266–276.

[20] V. P. Denysenkov, M. J. Prandolini, A. Krahn, M. Gafurov, B. Endeward, T. F. Prisner, *Appl. Magn. Reson.* **2008**, *34*, 289–299.

[21] A. A. Nevzorov, S. Milikisiyants, A. N. Marek, A. I. Smirnov, *J. Magn. Reson.* **2018**, *297*, 113–123.

[22] O. Nir-Arad, D. H. Shlomi, A. Israelstam, T. Amit, N. Manukovsky, A. B. Fialkov, I. Kaminker, *J. Magn. Reson.* **2024**, 107635.

[23] J. Granwehr, J. Forrer, A. Schweiger, *J. Magn. Reson.* **2001**, *151*, 78–84.

[24] A. Schweiger, R. R. Ernst, *J. Magn. Reson.* **1988**, *77*, 512–523.

[25] A. Himmler, M. M. Albannay, G. Von Witte, S. Kozerke, M. Ernst, *Magn. Reson.* **2022**, 1–12.

[26] I. Nicholson, F. J. L. Robb, D. J. Lurie, *J. Magn. Reson. Ser. B* **1994**, *104*, 284–288.

[27] A. Bornet, J. Milani, B. Vuichoud, A. J. Perez Linde, G. Bodenhausen, S. Jannin, *Chem. Phys. Lett.* **2014**, *602*, 63–67.

[28] X. Tang, S. Suddarth, G. Qian, M. Garwood, *J. Magn. Reson.* **2020**, *321*, 106855.

[29] G. Whitfield, A. G. Redfield, *Phys. Rev.* **1957**, *106*, 918–920.

[30] A. Capozzi, M. Karlsson, J. R. Petersen, M. H. Lerche, J. H. Ardenkjaer-Larsen, *J. Phys. Chem. C* **2018**, *122*, 7432–7443.

[31] D. Kurzbach, S. Jannin, **2018**, *7*, 117–132.

[32] T. Dubroca, A. N. Smith, K. J. Pike, S. Froud, R. Wylde, B. Trociewitz, J. McKay, F. Mentink-Vigier, J. van Tol, S. Wi, et al., *J. Magn. Reson.* **2018**, *289*, 35–44.

[33] V. S. Bajaj, M. K. Hornstein, K. E. Kreischer, J. R. Sirigiri, P. P. Woskov, M. L. Mak-Jurkauskas, J. Herzfeld, R. J. Temkin, R. G. Griffin, *J. Magn. Reson.* **2007**, *189*, 251–279.

[34] A. K. Hassan, L. A. Pardi, J. Krzystek, A. Sienkiewicz, P. Goy, M. Rohrer, L. C. Brunel, *J. Magn. Reson.* **2000**, *142*, 300–312.

[35] V. D. Arp, R. D. Mccarty, *Thermophysical Properties of Helium-4 from 0.8 to 1500 K with Pressures to 2000 MPa*, **1989**.

[36] R. D. Mc Carty, *J. Phys. Chem. Ref. Data* **1973**, *2*, 923–1042.

[37] M. Rosay, M. Blank, F. Engelke, *J. Magn. Reson.* **2016**, *264*, 88–98.

[38] E. L. Dane, T. Maly, G. T. Debelouchina, R. G. Griffin, T. M. Swager, *Org. Lett.* **2009**, *11*, 1871–1874.

[39] M. Baudin, B. Vuichoud, A. Bornet, G. Bodenhausen, S. Jannin, *J. Magn. Reson.* **2018**, *294*, 115–121.

[40] I. Kaminker, D. Shimon, Y. Hovav, A. Feintuch, S. Vega, *Phys. Chem. Chem. Phys.* **2016**, *18*, 11017–11041.

[41] S. Stoll, A. Schweiger, *J. Magn. Reson.* **2006**, *178*, 42–55.

[42] M. Florent, I. Kaminker, V. Nagarajan, D. Goldfarb, *J. Magn. Reson.* **2011**, *210*, 192–199.

[43] F. Mentink-Vigier, S. Vega, G. De Paëpe, *Phys. Chem. Chem. Phys.* **2017**, *19*, 3506–3522.

[44] W. T. Wenckebach, *J. Magn. Reson.* **2019**, *299*, 124–134.

[45] Z. Pang, S. Jain, C. Yang, X. Kong, K. O. Tan, *J. Chem. Phys.* **2022**, *156*, 244109.

[46] A. Schweiger, G. Jeschke, *Principles of Pulse Electron Paramagnetic Resonance*, Oxford University Press, **2002**.

[47] M. Blank, P. Borchard, S. Cauffman, K. Felch, M. Rosay, *Terahertz Sci. Technol.* **2016**, *9*, 177–186.

[48] T. V. Can, M. A. Caporini, F. Mentink-Vigier, B. Corzilius, J. J. Walish, M. Rosay, W. E. Maas, M. Baldus, S. Vega, T. M. Swager, et al., *J. Chem. Phys.* **2014**, *141*, 064202.

[49] X. Ji, T. V. Can, F. Mentink-Vigier, A. Bornet, J. Milani, B. Vuichoud, M. A. Caporini, R. G. Griffin, S. Jannin, M. Goldman, et al., *J. Magn. Reson.* **2018**, *286*, 138–142.

[50] M. Lelli, S. R. Chaudhari, D. Gajan, G. Casano, A. J. Rossini, O. Ouari, P. Tordo, A. Lesage, L. Emsley, *J. Am. Chem. Soc.* **2015**, *137*, 14558–14561.

[51] L. Delage-Laurin, R. S. Palani, N. Golota, M. Mardini, Y. Ouyang, K. O. Tan, T. M. Swager, R. G. Griffin, *J. Am. Chem. Soc.* **2021**, *143*, 20281–20290.

[52] A. Venkatesh, G. Casano, R. Wei, Y. Rao, H. Lingua, H. Karoui, M. Yulikov, O. Ouari, L. Emsley, *Angew. Chemie - Int. Ed.* **2024**, *202317337*, DOI 10.1002/anie.202317337.

[53] F. Mentink-Vigier, I. Marin-Montesinos, A. P. Jagtap, T. Halbritter, J. van Tol, S. Hediger, D. Lee, S. T. Sigurdsson, G. De Paëpe, *J. Am. Chem. Soc.* **2018**, *140*, 11013–11019.

[54] B. A. Rodin, V. Thalakottoor, M. Baudin, N. Birilirakis, G. Bodenhausen, A. V. Yurkovskaya, D. Abergel, *Phys. Chem. Chem. Phys.* **2023**, *25*, 15040–15051.

[55] T. Dubroca, X. Wang, F. Mentink-Vigier, B. Trociewitz, M. Starck, D. Parker, M. S. Sherwin, S. Hill, J. Krzystek, *J. Magn. Reson.* **2023**, *353*, 107480.

[56] A. Savitsky, K. Möbius, *Photosynth. Res.* **2009**, *102*, 311–333.

Supporting Information

EPR Simulation

The EPR simulation was performed using EasySpin (Stoll et. al., J. Magn. Resn. 178 (2006) 42-55) using the values adapted from the literature (Florent et. al., J. Magn. Resn. 210 (2011) 192-199). The MATLAB source code is given below:

```
Sys.g = [2.00878 2.00584 2.00204]; % g values
Exp.Field = 6702;          % static field, in mT
Exp.mwRange = [187.2 188.8];  % frequency range, in GHz
Sys.lwpp = 20; % linewidth

Sys.Nucs = '14N';          % one 14N nucleus
Sys.A = [2.05,2.17,9.8]*10;  % hyperfine principal values in MHz
Sys.Q=[-3.54 0.46];          % quadrupolar interaction, eeQq/h [MHz]

Exp.Temperature = 4.2; % temperature in kelvin
[Field,Spec] = pepper(Sys,Exp);       % returns the field axis and the spectrum
```

Observation of LOD-EPR Waveform

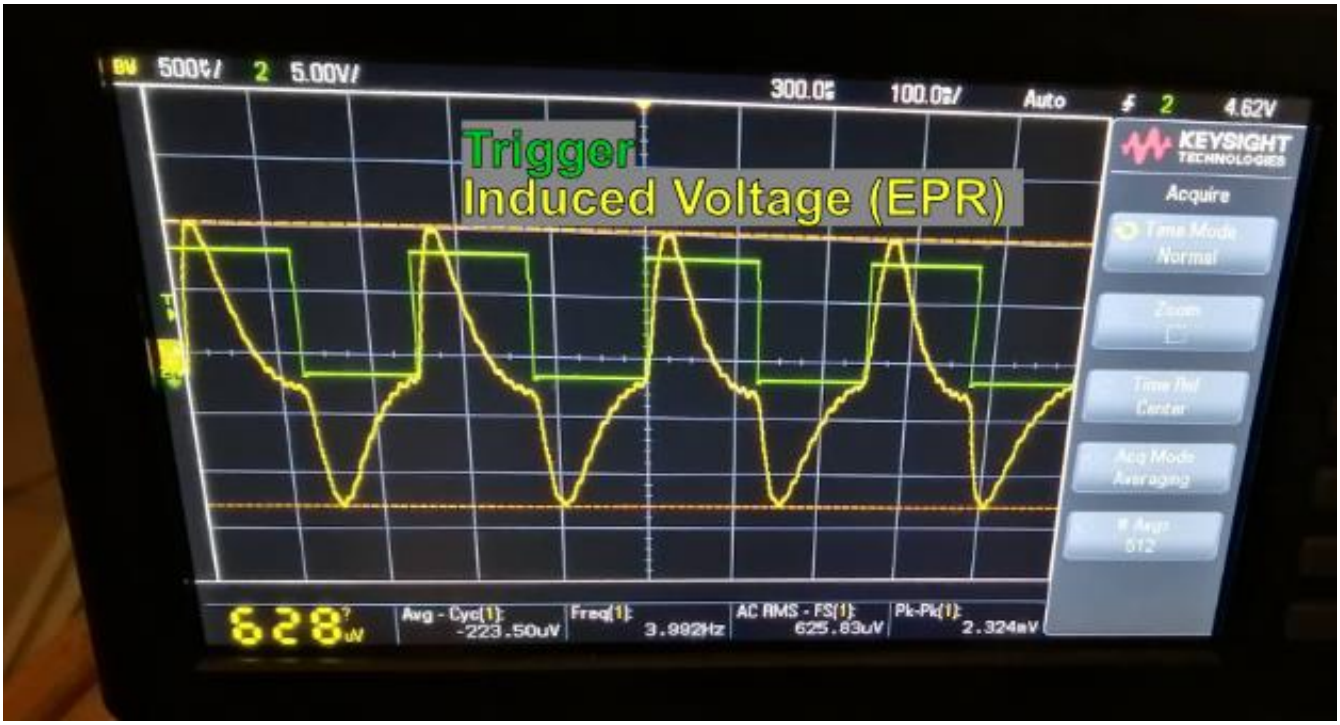

Figure S1: Direct detection of the LOD-EPR signal at the g_{yy} peak of TEMPOL at 4.2 K using an oscilloscope. The square-wave signal (green) shows the microwave on/off trigger, while the induced voltage (yellow) arises due to change in the EPR magnetization along the *z*-axis, i.e., $V(t) = \frac{dM_z(t)}{dt}$. A peak-to-peak voltage of ~2.3 mV (after pre-amplified by 10,000x) was recorded using 4 Hz microwave amplitude modulation (125 ms μw on and 125 ms μw off) and an average of 512 scans (total acquisition time ~ 8.5 minute).

Bypassing the interlock system in Gyrotron

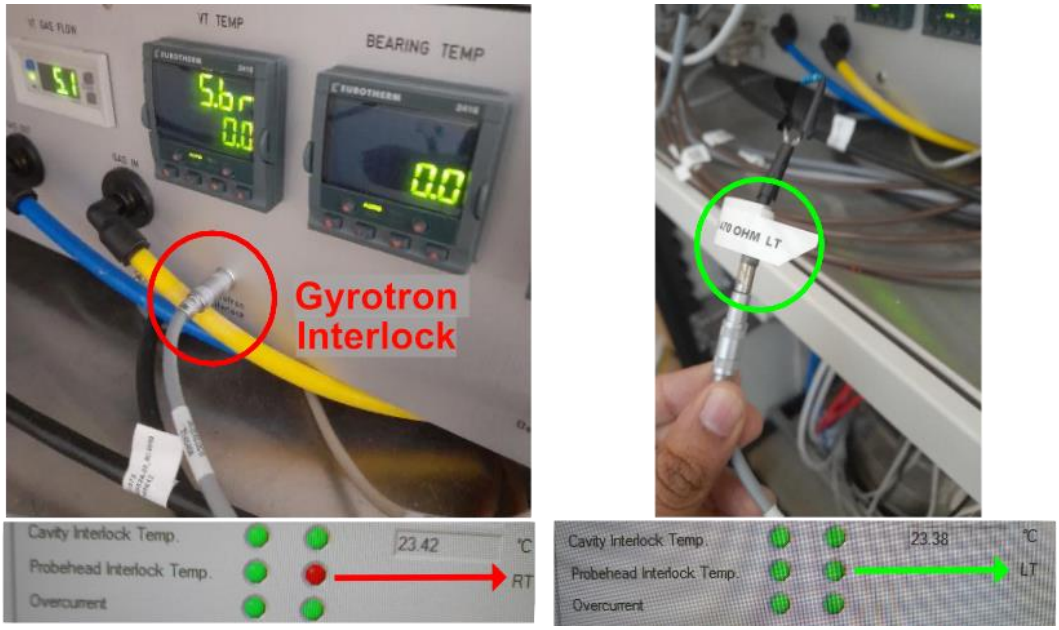

Figure S2: A 470 Ω resistor is used to bypass the gyrotron interlock system so that the gyrotron can be turned on irrespective of the probe temperature.

DNP Probe adapted with a 3D-printed housing

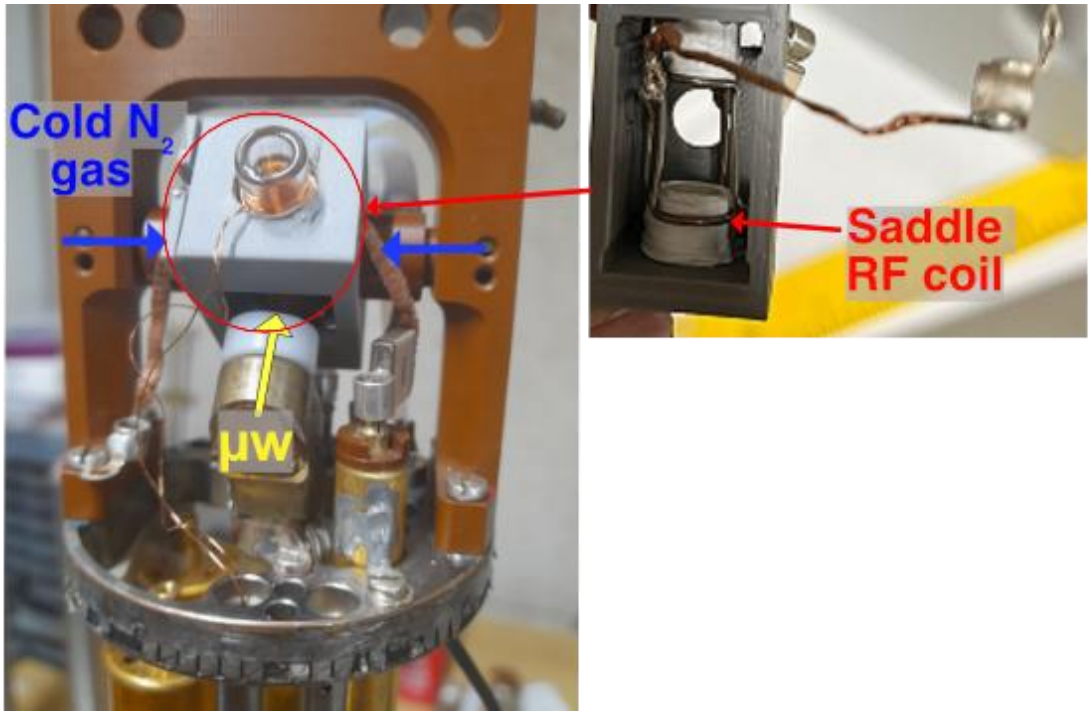

Figure S3: A modified commercial DNP probe with the 3.2 mm MAS stator replaced by a 3D-printed housing that hosts an LOD-EPR coil, a saddle rf coil, and a 7-mm NMR tube.